IOP PUBLISHING PLASMA PHYSICS AND CONTROLLED FUSION

Plasma Phys. Control. Fusion **49** (2007) B163–B172 doi:10.1088/0741-3335/49/12B/S15

Global gyrokinetic particle simulations with kinetic electrons

Z Lin, Y Nishimura, Y Xiao, I Holod, W L Zhang and L Chen

Department of Physics and Astronomy, University of California, Irvine, CA 92697, USA

E-mail: zhihongl@uci.edu

Received 6 July 2007
Published 15 November 2007
Online at stacks.iop.org/PPCF/49/B163

Abstract

A toroidal, nonlinear, electrostatic fluid-kinetic hybrid electron model is formulated for global gyrokinetic particle simulations of driftwave turbulence in fusion plasmas. Numerical properties are improved by an expansion of the electron response using a smallness parameter of the ratio of driftwave frequency to electron transit frequency. Linear simulations accurately recover the real frequency and growth rate of toroidal ion temperature gradient (ITG) instability. Trapped electrons increase the ITG growth rate by mostly not responding to the ITG modes. Nonlinear simulations of ITG turbulence find that the electron thermal and particle transport are much smaller than the ion thermal transport and that small scale zonal flows are generated through nonlinear interactions of the trapped electrons with the turbulence.

1. Introduction

Understanding and controlling ion thermal transport in fusion plasmas have been steadily improved thanks to orchestrated efforts in experiment, theory and simulation [1], in particular, intense studies of ion temperature gradient (ITG) turbulence [2]. Therefore, studying electron thermal transport as well as particle and momentum transport has become a high priority. First-principles simulations of electron thermal and particle transport need to treat kinetic effects of electrons. In the asymptotic limit of infinitely large thermal velocity as compared with the wave phase velocity, electrons can be modeled as adiabatic [3] in electrostatic gyrokinetic particle simulations [4] of ion transport driven by the ITG turbulence in tokamaks to avoid computational constraints due to the fast parallel motion of thermal electrons. However, the electrostatic adiabatic model cannot treat the electron parallel and precessional resonances, the nonadiabatic response of magnetically trapped electrons and the nonresonant current of thermal electrons.

Direct implementation of the electron drift kinetic equation in gyrokinetic particle simulations of tokamak plasmas introduces stringent numerical constraints associated with

enhanced discrete particle noise [5], electron parallel Courant condition [6], high-frequency electrostatic oscillation (the so-called ω_H mode) [4] and electromagnetic fluctuation with tearing parity near mode rational surfaces [7, 8]. Recognizing that the electron response in the driftwave and Alfvenic turbulence is dominated by the adiabatic component, a split-weight scheme in the slab geometry [9] was introduced to separate the electron response into an adiabatic part and a nonadiabatic part, which has been implemented in some gyrokinetic toroidal particle codes [10, 11]. Since the adiabatic component can be described analytically, simulation only needs to treat the non-adiabatic component, an approach similar to the analytic gyrokinetic theory [12]. The advantage of the split-weight scheme is to remove the particle noise associated with the electron adiabatic response [13], while retaining all the physics associated with the kinetic electrons. However, since it is an exact formulation of the drift kinetic equation, the Courant condition, the high-frequency ω_H mode in electrostatic simulation and the tearing mode in electromagnetic simulation still place stringent numerical constraints [14].

The concept of treating only the nonadiabatic component dynamically leads to the development of a fluid-kinetic hybrid electron model [15] in the slab geometry, which has been extended to the toroidal geometry and implemented in the gyrokinetic toroidal code (GTC) [16]. In this hybrid model, electron response is asymptotically expanded order by order based on a smallness parameter of the ratio of wave phase velocity to electron thermal velocity. In the lowest order, electron response is adiabatic and is thus treated as a massless fluid commonly employed in space plasma physics [17]. The nonresonant current is fully retained in the electron fluid equations without the need to resolve the dynamics of thermal electrons, i.e. the electron Courant condition can be circumvented. In fact, the ideal magnetohydrodynamic (MHD) dispersion of shear Alfven wave in tokamak has been recovered in electromagnetic GTC simulations [16] using the lowest order hybrid expansion with adiabatic electrons. The dynamics of kinetic electrons is implemented perturbatively as higher order corrections to treat the electron parallel and precessional resonances and the nonadiabatic response of magnetically trapped electrons. Since electrons behave as a 'frozen-in-line' massless fluid [14] in the lowest order expansion, the magnetic topology is preserved. The electron resonance with the perturbation of the tearing parity near mode rational surfaces and the tearing mode are thus systematically removed by the expansion ordering. Therefore, the well-known difficulty [7, 8] of resolving the electron resonance with tearing parity near mode rational surfaces is eliminated. Furthermore, the high-frequency ω_H mode in electrostatic simulation is also removed from the hybrid model [15]. The improvement of numerical properties comes from the approximation made in the expansion of the electron response, i.e. the hybrid model is not an exact formulation of the electron drift kinetic equation. The price to pay for the improved numerical properties is that the model cannot treat the tearing mode physics. However, the hybrid model is most suitable for simulations of the driftwave turbulence and MHD turbulence for studying electron transport and energetic particle physics. The hybrid model retains rigorously linear and nonlinear electron resonances with Alfvenic and ion acoustic waves such as the Alfven-ion temperature gradient (AITG) [18] mode and the toroidal Alfven eigenmode (TAE) [19].

The electromagnetic version of the hybrid electron model uses the ratio of the Alfvenic/ion acoustic wave phase velocity to the electron thermal velocity as the smallness parameter for the expansion of the electron response [16]. In the electrostatic toroidal simulation, the smallness parameter is the ratio of the driftwave frequency to the electron transit frequency. The toroidal formulation and GTC implementation of the electrostatic hybrid electron model is presented in section 2. In section 3, GTC simulations of ITG instability and turbulence with kinetic electrons are presented. The linear dispersion relation is found to agree well with an eigenvalue code and another gyrokinetic particle code. The increase in ITG growth rate is shown to result

from nearly no response (i.e. nonadiabatic) of trapped electrons to the ITG modes. Linear poloidal coupling is shown to prevent a singular electron response near mode rational surfaces in electrostatic ballooning modes [20]. Nonlinear simulations indicate that electron thermal transport in the ITG turbulence is driven by nonresonant interactions. Both the particle transport and the electron thermal transport are much smaller than the ion thermal transport in the ITG turbulence. Short scale zonal flows are generated by nonlinear interactions of trapped electrons with the ITG turbulence. Conclusions are drawn in section 4. Application of the hybrid electron model for simulation of TEM turbulence will appear in a separate paper.

2. Nonlinear electrostatic fluid-kinetic hybrid electron mode in toroidal geometry

We consider a simple plasma of electrons and ions. Assuming the wavelength of electrostatic fluctuations is much longer than the electron gyroradius, the dynamics of electrons is governed by the electron guiding center Hamiltonian in the phase space of ($\boldsymbol{x}$,μ, $v_{||}$), where $\boldsymbol{x}$ is the 3D real space, μ is the magnetic moment and $v_{||}$ is the parallel velocity,

$$H = \tfrac{1}{2} m_{\mathrm{e}} v_{\|}^2 + \mu B - e\phi$$

with B the magnetic field amplitude, m_{e} the electron mass, e the magnitude of electron charge and ϕ the electrostatic potential. The electron drift kinetic equation in ($\boldsymbol{x}$,μ, $v_{\|}$) space is,

$$\left[\frac{\partial}{\partial t} + \left(v_{\|}\boldsymbol{b} + \boldsymbol{v}_{\mathrm{d}} + \boldsymbol{v}_E\right)\cdot\frac{\partial}{\partial \boldsymbol{x}} - \boldsymbol{b}^*\cdot\nabla(\mu B - e\phi)\frac{\partial}{m_{\mathrm{e}}\partial v_{\|}} - C_{\mathrm{e}}\right] f_{\mathrm{e}} = 0, \qquad (1)$$

where $\boldsymbol{b}^* = \boldsymbol{b} - (m_{\mathrm{e}} c v_{||}/eB^*)\boldsymbol{b}\times(\boldsymbol{b}\cdot\nabla\boldsymbol{b})$, $\boldsymbol{v}_{\mathrm{d}} = -(c/eB^*)\boldsymbol{b}\times(\mu\nabla B + m_{\mathrm{e}} v_{\|}^2 \boldsymbol{b}\cdot\nabla\boldsymbol{b})$, $\boldsymbol{v}_E = (c/B^*)\boldsymbol{b}\times\nabla\phi$, $\boldsymbol{b} = \boldsymbol{B}/B$, $B^* = B - (m_{\mathrm{e}} c v_{||}/e\boldsymbol{b})\cdot\nabla\times\boldsymbol{b}$ and c is the speed of light. The appearance of B^* ensures that the guiding center drifts preserve the Hamiltonian structure. A collision operator C_{e} is added to represent electron–electron and electron–ion collisions. The ion dynamics is governed by the nonlinear gyrokinetic equation that also preserves the Hamiltonian structure [21, 22].

The electrostatic potential is derived from the gyrokinetic Poisson equation [4],

$$\frac{\tau}{\lambda_{\mathrm{D}}^2}\left(\phi - \tilde{\phi}\right) = 4\pi e(\delta\bar{n}_{\mathrm{i}} - \delta n_{\mathrm{e}}),$$

where $\tau = T_{\mathrm{e}}/T_{\mathrm{i}}$ is the ratio of electron to ion temperature, $\lambda_{\mathrm{D}}^2 = T_{\mathrm{e}}/4\pi n_0 e^2$ is the Debye length, n_0 is the equilibrium electron density and the tilde represents double-gyroaveraging [4]. For electrostatic driftwave turbulence, the zonal flow component ($k_{||} = 0$) is much larger than the nonzonal flow component [3]. Electron responses to the two components are quite different: nearly adiabatic response to the non-zonal component and nearly no response to the zonal flows. Therefore, it is numerically advantageous to solve the two components separately by writing $\phi = \langle\phi\rangle + \delta\phi$, where the angle bracket represents the flux-surface averaging. Here we take a high aspect-ratio limit so that the double-gyroaveraging and flux-surface averaging are commutable.

We now expand the electron response and the electrostatic potential using a smallness parameter of $\delta = \omega/\omega_{\mathrm{e}} \ll 1$, where ω is the mode frequency and ω_{e} is the electron transit frequency, $f_{\mathrm{e}} = f_{\mathrm{e}0}\mathrm{e}^{e\delta\phi/T_{\mathrm{e}}} + \delta g_{\mathrm{e}}^{(1)}$, and $\delta\phi = \delta\phi^{(0)} + \delta\phi^{(1)}$, where the nonadiabatic parts $\delta g_{\mathrm{e}}^{(1)}$ and $\delta\phi^{(1)}$ are smaller than the adiabatic parts by a factor of δ. The electron equilibrium is defined as

$$\left[\left(v_{\|}\boldsymbol{b} + \boldsymbol{v}_{\mathrm{d}}\right)\cdot\frac{\partial}{\partial \boldsymbol{x}} - \boldsymbol{b}^*\cdot\nabla(\mu B)\frac{\partial}{m_{\mathrm{e}}\partial v_{\|}} - C_{\mathrm{e}}\right] f_{\mathrm{e}0} = 0.$$

The solution of f_{e0} is the neoclassical equilibrium. Here we approximate f_{e0} as a local Maxwellian.

In the lowest order, electron response is adiabatic,

$$\frac{\delta n_e}{n_0} = e^{e\delta\phi^{(0)}/T_e} - 1.$$

The gyrokinetic Poisson equation for the lowest order nonzonal component $\delta\phi^{(0)}$ becomes

$$\frac{(\tau+1)e\delta\phi^{(0)}}{T_e} - \frac{\tau e\delta\tilde{\phi}^{(0)}}{T_e} = \frac{\delta\bar{n}_i - \langle\delta\bar{n}_i\rangle}{n_0} \tag{2}$$

with $\delta\bar{n}_i = \int \delta f_i\, d^3\boldsymbol{v}$ with the perturbed ion distribution function $\delta f_i = f_i - f_{i0}$. In the initial value simulation, particle orbits and fields are updated in a sequence of time stepping. At the jth time step with all field quantities known, ion orbits are pushed to the $(j+1)$th time step using the ion gyrokinetic equation [22]. The lowest order solution of the nonzonal component of the electrostatic potential is obtained at the $(j+1)$th time step from equation (2) using an iterative [23] or a finite element method [24].

In the higher order, the dynamics of electrons is treated using the drift kinetic equation of $\delta g_e^{(1)}$,

$$\begin{aligned}\left[\frac{\partial}{\partial t} + \left(v_\parallel\boldsymbol{b} + \boldsymbol{v}_d + \boldsymbol{v}_E\right)\cdot\frac{\partial}{\partial\boldsymbol{x}} - \boldsymbol{b}^*\cdot\nabla(\mu B - e\phi)\frac{\partial}{m_e\partial v_\parallel} - C_e\right]\delta g_e^{(1)} \\ = -f_{e0}e^{e\delta\phi/T_e}\left[\frac{\partial}{\partial t}\left(\frac{e\delta\phi^{(0)}}{T_e}\right) + \delta\boldsymbol{v}_E\cdot\nabla\left(\ln f_{e0}\right)_{|v_\parallel,v_\perp}\right. \\ \left. -\left(\boldsymbol{v}_d + \delta\boldsymbol{v}_E\right)\cdot\nabla\left(\frac{e\langle\phi\rangle}{T_e}\right)\right],\end{aligned} \tag{3}$$

where $\delta\boldsymbol{v}_E = (c/B^*)\boldsymbol{b}\times\nabla\delta\phi$, and the gradient operator on f_{e0} in the second term on the right-hand side is taken with $v_\parallel$, $v_\perp$held fixed. The equilibrium pressure gradient scale length is assumed to be much longer than the perturbation wavelength. The first two terms on the right-hand side are the familiar ω and $\omega*$ terms, respectively, and the third term is the convection of zonal flows by magnetic and $\boldsymbol{E}\times\boldsymbol{B}$ drifts. Equation (3) is an approximate equation since we replace the exact potential $\delta\phi$ with the lowest order solution $\delta\phi^{(0)}$ in the first term on the right-hand side. This approximation is required for numerical stability when taking the time-derivative for the first term on the right-hand side, i.e. a time-centered operation for the jth time step by using the lowest order solutions at the $(j+1)$th and $(j-1)$th time steps. Physically, this approximation renders electron response inaccurate near mode rational surfaces (where $k_\parallel \to 0$), since the lowest order solution $\delta\phi^{(0)}$ does not dominate there. Electron orbits are now pushed from the jth time step to the $(j+1)$th time step using all field quantities at the jth time step in equation (3). The electrostatic potential with the first order correction at the $(j+1)$th time step becomes:

$$e^{e\delta\phi/T_e} = e^{e\delta\phi^{(0)}/T_e} - \frac{\delta n_e^{(1)} - \langle\delta n_e^{(1)}\rangle}{n_0} \tag{4}$$

with $\delta n_e^{(1)} = \int \delta g_e^{(1)}\, d^3\boldsymbol{v}$. Equations (3) and (4) can be repeated to reach higher orders in the expansion of the electron response. In the toroidal system, the response of magnetically trapped electrons is not dominantly adiabatic. Higher order expansion is needed depending on the trapped fraction. We found that the second order expansion is sufficiently accurate for typical values of the tokamak aspect-ratio (see section 3).

After all particle orbits and nonzonal components of field quantities are updated to a desired accuracy at the $(j+1)$th time step, the zonal flows at the $(j+1)$th time step are calculated from

$$\frac{\tau e\left(\langle\phi\rangle - \langle\tilde{\phi}\rangle\right)}{T_e} = \frac{\langle\delta\bar{n}_i\rangle - \langle\delta n_e^{(1)}\rangle}{n_0}. \tag{5}$$

The cycle of equations (2)–(5) can then be repeated to the next time step.

3. Global simulation of ITG turbulence with kinetic electrons

The nonlinear, electrostatic kinetic-fluid hybrid electron model described in section 2 has been implemented in the GTC [3], which is a well-benchmarked, massively parallel, global gyrokinetic particle-in-cell code incorporating both linear and nonlinear wave–particle interactions and nonlocal geometric effects. A global field-aligned mesh [25] provides the maximal computational efficiency without any approximation in physics or geometry to describe the toroidal eigenmode with anisotropic structures. An effective collision operator modeling a heat bath [26] prevents the relaxation of the temperature profile. The tokamak with concentric flux-surfaces is described by magnetic coordinates (r, θ, ζ), where r is the radial coordinate labeling the flux-surfaces, θ is the poloidal angle and ζ is the toroidal angle. These global GTC simulations use representative tokamak plasmas with the following local parameters at a radial position $r = 0.5a$, $R/L_{Te} = 6.9$, $R/L_n = 2.2$, $q = 1.4$, s=0.78, $T_e/T_i = 1$ and $a/R = 0.36$. Here R and a are the major and minor radii, L_{Te} and L_n are the electron temperature and density gradient scale lengths, T_i and T_e are the ion and electron temperatures, q is the safety factor and s is the magnetic shear. The profile for the safety factor is $q = 0.581 + 1.092(r/a) + 1.092(r/a)^2$ and for the temperature and density gradients is $\exp\{-[(r-0.5a)/0.32a]^6\}$. Collisions are not treated in present simulations. The boundary condition of the perturbed electrostatic potential $\phi = 0$ is enforced at $r < 0.1a$ and $r > 0.9a$. The size of the tokamak used in the simulation is $a = 250\rho_i$ for nonlinear simulations and $a = 125\rho_i$ for linear simulations, where $\rho_i = v_i/\Omega_i$ is the ion gyroradius, ion thermal speed$v_i = (T_i/m_i)^{1/2}$ and ion mass m_i. The computational mesh consists of 32 toroidal grids and a set of unstructured radial and poloidal grids with a perpendicular grid size of ρ_i. The time step is $0.2L_{Te}/v_i$.

To verify the electrostatic hybrid electron model for simulations of driftwave instabilities such as ITG or trapped electron mode (TEM) instability, linear simulation was first carried out. A key issue of numerical convergences is which order in the expansion of the electron response is sufficient to recover the dynamics of magnetically trapped electrons. Since TEM instability is the most sensitive to the response of trapped electrons, we performed the convergence test for the TEM mode by using a parameter of the ITG with $R/L_{Ti} = 1.1$, which excites the TEM mode but not the ITG mode. Shown in figure 1(a) is the dependence of the real frequency and the growth rate of the TEM mode with $k_{\theta\rho i} = 0.335$ on the order of the expansion in the hybrid electron model. Clearly, the second order expansion is sufficiently accurate even though the trapped fraction is about 42%. This is probably due to the fact that the real frequency of the toroidal driftwave eigenmodes is primarily determined by the combination of diamagnetic frequency ($\omega*$) and drift frequency (ω_d), but insensitive to the electron response (see figure 3). In all simulations presented in the rest of this paper, electron response is treated to the second order expansion of the hybrid model.

The ITG is varied to investigate the relative drive for the TEM and ITG modes. Shown in figure 1(b) is the dependence on the ITG of the real frequency and the growth rate of a toroidal eigenmode with $k_\theta \rho i = 0.335$, which typically has the highest growth rate for the

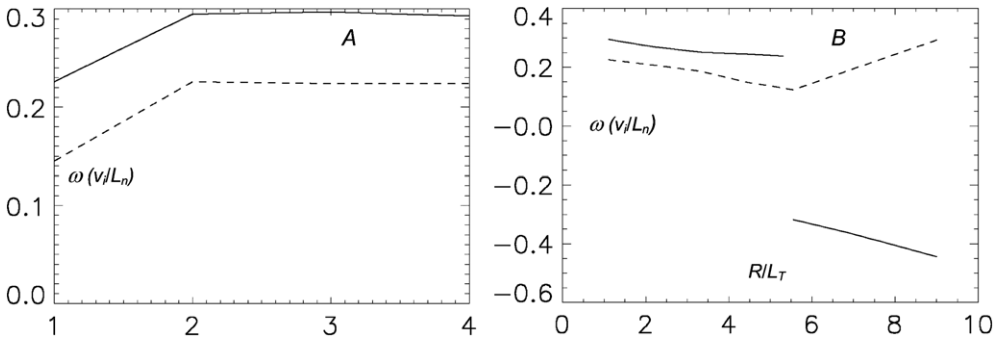

Figure 1. Dependence of frequency (solid) and growth rate (dashed) on the order of expansion in the hybrid electron model for $R/L_{\mathrm{Ti}} = 1.1$ (*a*) and on the ion temperature gradient (*b*).

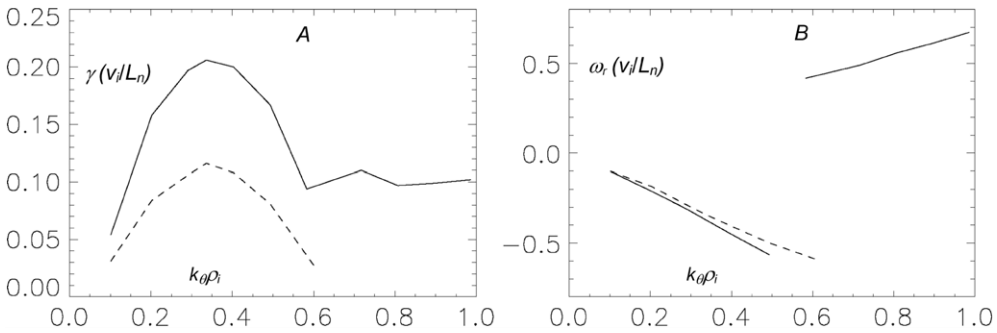

Figure 2. Dependence of growth rate (*a*) and frequency (*B*) on poloidal wavelength for $R/L_{\mathrm{Ti}} = 6.9$. The solid lines are for kinetic electrons and the dashed lines are for adiabatic electrons.

ITG modes. For small ITG, $R/L_{\mathrm{Ti}} < 5.5$, the TEM instability has a higher growth rate as the real frequency is positive, which means that the wave phase velocity is in the electron diamagnetic drift direction. For stronger ITGs, $R/L_{\mathrm{Ti}} > 5.5$, the ITG instability has a higher growth rate as the real frequency becomes negative. To examine the response of passing electrons, simulations with both passing and trapped electrons are compared with simulations with trapped electrons only. The differences in the frequency and the growth rate are found to be less than 1%, indicating that the response of the passing electrons is very close to adiabatic. Therefore, only trapped electrons are kept in all simulations reported in the rest of this paper.

We now focus on the regime of a strong ITG with $R/L_{\mathrm{Ti}} = 6.9$. Shown in figure 2 is the dependence of the growth rate and the frequency on the poloidal wavelength for simulations with kinetic electrons and with adiabatic electrons, respectively. When the electron response is adiabatic, only the ITG modes are unstable (real frequency is negative) for the range of poloidal wavelength $k_\theta \rho_{\mathrm{i}} < 0.6$. With non-adiabatic electrons, the growth rate of the most unstable ITG mode increases by almost a factor of 2, and short-wavelength TEM modes are found to be unstable with a higher growth rate than that of the ITG modes for $k_\theta \rho_{\mathrm{i}} > 0.6$. The co-existence of both the ITG and the TEM modes has been reported earlier [27]. All GTC results of figures 1 and 2 are found to agree well with a comprehensive toroidal eigenvalue code FULL and another gyrokinetic particle code GT3D [28].

The increase of the ITG growth rate when trapped electrons are included in the simulations has previously been observed. This is generally attributed to the nonadiabatic response of the

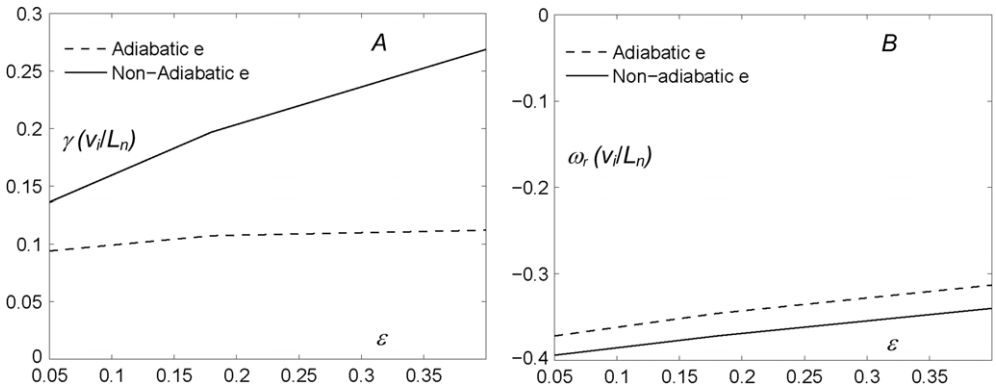

Figure 3. Dependence of growth rate (a) and frequency (b) on inverse aspect-ratio $\varepsilon = a/R$ with $r = 0.5a$ and $R/L_{\mathrm{Ti}} = 6.9$. The solid lines are for kinetic electrons and the dashed lines are for adiabatic electrons.

trapped electrons. However, since the toroidal precession of the trapped electrons is in the opposite direction of the ITG phase velocity, trapped electrons do not interact resonantly with the ITG modes. To elucidate the physical mechanism of the enhancement of the ITG growth rate by the trapped electrons, the inverse aspect-ratio is varied while all other dimensionless quantities are kept constant to examine the dependence of the ITG frequency and the growth rate on the fraction of trapped particles. As shown in figure 3, when the electron response is adiabatic, the ITG frequency and growth rate are insensitive to the inverse aspect-ratio. This is due to the fact that the ITG frequency is faster than the ion bounce frequency so that the trapped ions play no special roles. On the other hand, when the dynamics of trapped electrons are treated in the simulation, the ITG growth rate increases with the fraction of the trapped electrons even though the frequency is insensitive to the trapped fraction. This is consistent with the fact that the ITG frequency is determined by a combination of the ion diamagnetic and drift frequencies to satisfy a resonant condition with ions, so that it is insensitive to the electron response. Since the trapped electrons do not interact resonantly with the ITG modes, the response of trapped electrons is nearly zero, rather than adiabatic. Therefore the dielectric constant in the gyrokinetic Poisson equation decreases when the trapped fraction increases, leading to a higher ITG growth rate. To confirm this physics picture, we have performed a linear simulation assuming the adiabatic response for the passing electrons and no response for the trapped electrons (i.e. $\delta n_{\mathrm{e}} = 0$ for trapped electrons). The growth rate is found to agree very well with the simulation with kinetic electrons.

The structure of the toroidal ITG eigenmode ($k_\theta \rho_{\mathrm{i}} = 0.335$) with kinetic electrons is shown in figure 4. The overlap is very strong between neighboring poloidal harmonics (i.e. m and $m \pm 1$), significant between $(m + 1)$ and $(m - 1)$ and insignificant further apart. Thus the mode is modestly ballooning. It is clear that the component of the $k_\parallel \to 0$ perturbation never appears at any mode rational surface because of the linear poloidal coupling in the presence of a finite magnetic shear. In particular, there is no singular behavior at the low-order mode rational surfaces of $q = 1, 1.5$ and 2, which appear at the radial positions of $r/a = 0.30$, 0.54 and 0.74, respectively. This is quite different from the sheared slab case, which allows the component of the $k_\parallel \to 0$ perturbation near the mode rational surface. This explains the good agreement [28] in the linear dispersion relation in the presence of the magnetic shear between the FULL eigenvalue code and the GTC simulation with the hybrid electron model.

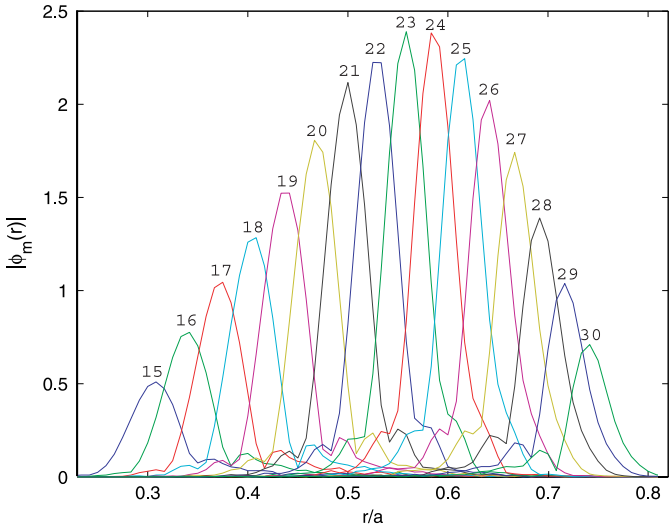

Figure 4. Radial structures of poloidal harmonics (m) for a toroidal eigenmode $n = 15$.

(Some figures in this article are in colour only in the electronic version)

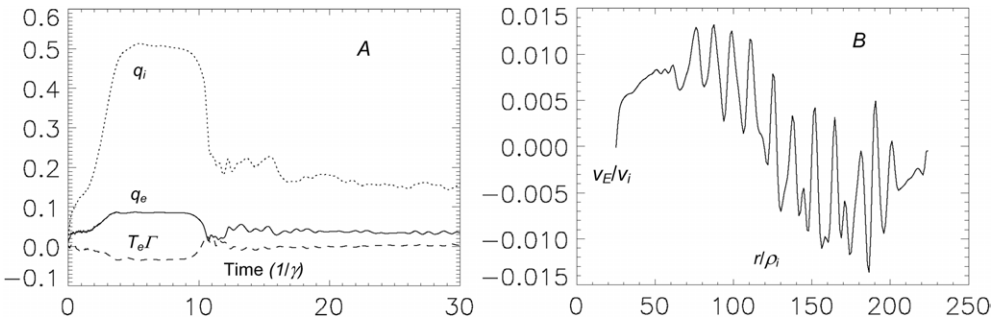

Figure 5. Time histories of ion heat flux q_i (dotted), electron heat flux q_e (solid), particle flux Γ (dashed), all normalized by fluctuation intensity $\langle \delta\phi^2 \rangle$ (*a*) and instantaneous radial profile of zonal flows normalized by ion thermal velocity (*b*).

With the rigorous linear benchmark, the hybrid electron model is now applied for nonlinear simulations of ITG-dominated turbulence with kinetic electrons using $R/L_{Ti} = 6.9$. Since the ITG frequency is much smaller than the bounce frequency of electrons, electrons are pushed 10 times for every time step of ion orbits and field solvers. Shown in figure 5(*a*) are volume-averaged time histories of ion heat flux electron heat flux, and particle flux, all normalized by the fluctuation intensity $\langle \delta\phi^2 \rangle$ from a simulation using 100 particles per cell. The ratio of transport to fluctuation intensity plotted in figure 5(*a*) indicates the strength of coherent wave–particle interactions, i.e. a measure of effective wave–particle decorrelation time [29]. After an initial phase of random fluctuations, linear eigenmodes are formed as demonstrated by the long wave–ion decorrelation time for a period of $3/\gamma < t < 10/\gamma$. This is due to the fact that ITG is driven by the ion resonance and the only decorrelation mechanism for ions in the linear phase is the growth rate. In contrast, the effective decorrelation time for electrons is much shorter during this linear phase. The instability saturates at $t \sim 10/\gamma$ and reaches

a quasi-steady state after $t \sim 16/\gamma$. In this saturation process, the poloidal spectrum shifts downward from ($k_\theta \rho_i \sim 0.3$) to ($k_\theta \rho_i \sim 0.15$) due to a spectral energy cascade induced by the nonlinear toroidal coupling [30,31]. The electron thermal transport is about a factor of 5 smaller than the ion thermal transport and the particle transport is even smaller. The fact that the ion and electron transport are different for the same fluctuation intensity indicates that the transport mechanisms for ions and electrons are different due to the different nature of wave–particle interactions. While the ion transport is governed by the wave–ion resonance, the electron transport is governed by nonresonant, nonlinear processes in ITG-dominated turbulence [32].

Another nonlinear feature of interest in the ITG-dominated turbulence with kinetic electrons is the generation of short-wavelength zonal flows ($k_r \rho_i \sim 0.5$), as shown in figure 5(*b*). For comparison, when the electron response is adiabatic, zonal flows are dominated by much longer wavelength modes ($k_r \rho_i \sim 0.1$) [33]. The generation of the short-wavelength zonal flows by kinetic electrons may suggest higher order nonlinear processes, e.g. ITG mode scattering off trapped electrons, in consistence with the nonresonant electron transport in the ITG-dominated turbulence. A comparison of resonant and nonresonant electron transport in ITG and TEM turbulence will be reported in a separate paper.

4. Conclusion

A toroidal, nonlinear, electrostatic fluid-kinetic hybrid electron model is formulated for global gyrokinetic particle simulations of the driftwave turbulence in fusion plasmas. Linear simulations accurately recover the real frequency and the growth rate of toroidal ITG instability. Trapped electrons enhance the ITG growth rate by mostly not responding to the ITG modes. Nonlinear simulations find that the electron thermal and particle transport are much smaller than the ion thermal transport and that small scale zonal flows are generated through nonlinear interactions of the trapped electrons with the ITG turbulence.

Acknowledgments

ZL gratefully acknowledges useful discussions with T S Hahm, P H Diamond and F Zonca. This work was supported by the US Department of Energy (DOE) Grant DE-FG02-07ER54916 and DE-FG03-94ER54736, Cooperative Agreement DE-FC02-04ER54796 and 06ER54860, and in part by SciDAC GPS and CPES. Simulations used supercomputers at NERSC and ORNL.

References

[1] Doyle E J *et al* 2007 *Nucl. Fusion* **47** S18
[2] Horton W 1999 *Rev. Mod. Phys.* **71** 735
[3] Lin Z 1998 *et al Science* **281** 1835
[4] Lee W W 1987 *J. Comput. Phys.* **72** 243
[5] Birdsall C K and Langdon A B 1985 *Plasma Physics via Computer Simulation* (New York: McGraw-Hill)
[6] Sydora R D, Decyk V K and Dawson J M 1996 *Plasma Phys. Control. Fusion* **38** A281
[7] Reynders J C 1992 *PhD Dissertation* Princeton University
[8] Cummings J C 1995 *PhD Dissertation* Princeton University
[9] Manuilskiy I and Lee W W 2000 *Phys. Plasmas* **7** 1381
[10] Chen Y and Parker S E 2003 *J. Comput. Phys.* **189** 463
[11] Lewandowski J L V *et al* 2006 *Phys. Plasmas* **13** 072306
[12] Frieman E A and Chen L 1982 *Phys. Fluids* **25** 502
[13] Lee W W *et al* 2001 *Phys. Plasmas* **8** 4435
[14] Hinton F L, Rosenbluth M N and Waltz R E 2003 *Phys. Plasmas* **10** 168

[15] Lin Z and Chen L 2001 *Phys. Plasmas* **8** 1447
[16] Nishimura Y, Lin Z and Wang W X 2007 *Phys. Plasmas* **14** 042503
[17] Lin Y and Swift D W 1996 *J. Geophys. Res.-Space Phys.* **101** 19859
[18] Zonca F *et al* 1998 *Plasma Phys. Control. Fusion* **40** 2009
[19] Cheng C Z, Chen L and Chance M S 1985 *Ann. Phys.* (N. Y.) **161** 21
[20] Romanelli F and Zonca F 1993 *Phys. Fluids* B **5** 4081
[21] Hahm T S 1988 *Phys. Fluids* **31** 2670
[22] Brizard A J and Hahm T S 2007 *Rev. Mod. Phys.* **79** 421
[23] Lin Z and Lee W W 1995 *Phys. Rev.* E **52** 5646
[24] Nishimura Y *et al* 2006 *J. Comput. Phys.* **214** 657
[25] Lin Z *et al* 2002 *Phys. Rev. Lett.* **88** 195004
[26] Lin Z and Hahm T S 2004 *Phys. Plasmas* **11** 1099
[27] Dong J Q, Mahajan S M and Horton W 1997 *Phys. Plasmas* **4** 755
[28] Rewodlt G, Lin Z and Idomura Y 2007 *Comput. Phys. Commun.* at press
[29] Lin Z *et al* 2007 *Phys. Rev. Lett.* submitted
[30] Lin Z, Chen L and Zonca F 2005 *Phys. Plasmas* **12** 056125
[31] Chen L, Zonca F and Lin Z 2005 *Plasma Phys. Control. Fusion* **47** B71
[32] Similon P L and Diamond P H 1984 *Phys. Fluids* **27** 916
[33] Hahm T S *et al* 2000 *Phys. Control. Fusion* **42** A205